On the importance of weak steady shear in the refraction of short internal waves

Greg Buckley,[1] Dave Broutman,[1,2,3] James W. Rottman,[4] and Stephen Eckermann[3]

Abstract. Ray theory is used to study the refraction of short oceanic internal waves by a spectrum of large amplitude inertia waves superimposed on a weakly sheared steady current. The results suggest that the steady current has a significant cumulative effect on short-wave propagation over the timescale of a few inertia periods. The strength of ray convergence is also computed, as this affects short-wave amplitudes. Typically we find weak ray convergence and much slower growth toward instability with increasing vertical wavenumber than in a steady-shear critical-layer model.

1. Introduction

Much of the mixing in the ocean's interior is believed to be triggered by breaking internal waves of short vertical wavelength, typically a few meters (e.g. [*Gregg et al*, 1996]). Refraction may play an important role in bringing internal waves to such short scales and to unstable amplitudes, as suggested by the results of [*Henyey, Wright and Flatte*, 1986] (hereafter HWF). Their model, based partly on Monte-Carlo ray tracings, produces short-wave spectra and mixing rates that are roughly comparable with ocean measurements.

HWF predict mixing rates by estimating the net transport, due to refraction, of wave-energy across the high-wavenumber part of the internal-wave spectrum. Here we examine two aspects of short-wave refraction that can affect net transport and that are not explicitly taken into account by HWF.

The first aspect is the effect of steady shear. In HWF, the short waves are refracted by a Garrett-Munk background of longer internal waves, without steady shear. Although steady shear in the ocean is typically much weaker than the *rms* internal-wave shear, it can have a significant cumulative effect on short-wave refraction, decreasing the time it takes to refract to very short scales. Using ray tracing, we illustrate this by following groups of short internal waves through a combination of large-amplitude inertia waves and a weakly sheared steady current.

The second aspect is the effect of ray convergence. While the presence of steady shear enhances the transport of wave-energy toward small scales, the strength of ray convergence can influence transport toward larger scales. This is because

the weaker the ray convergence the less likely the short waves are to reach unstable amplitudes and the more likely they are to refract back to larger scale for another cycle of the inertia oscillation. Here we find a range of convergence strengths at small scale, but mostly we find weak convergence, especially compared to convergence in a critical-layer model.

2. Model Formulation

The inertia frequency f and the buoyancy frequency N are constant, with $f = 10^{-4}s^{-1}$ and $N = 26f$, the latter taken from the Garrett-Munk model for a depth of about $1000m$ below the sea surface. Cartesian coordinates are used with z positive upwards. The background velocity $\mathbf{U} = (U, V, 0)$ consists of a random combination of inertia waves and a steady geostrophic current Rz:

$$U + iV = e^{-ift} \sum_{n=1}^{NW} U_n e^{i\phi_n} \sin(M_n z) + Rz \qquad (1)$$

where R is a real constant, $NW = 250$ is the number of inertia waves, and ϕ_n is a random phase evenly distributed between 0 and 2π. The vertical wavenumbers $M_n = n\pi/B$, where $B = 1300m$ is the buoyancy-frequency depth scale in the Garrett-Munk model. The amplitudes U_n are chosen to give a vertical-wavenumber spectrum for horizontal velocity that has the same shape as that of Garrett-Munk ([*Munk*, 1981]), but is scaled to give an *rms* horizontal velocity of $4cm\ s^{-1}$, or an *rms* inverse Richardson number of 0.7. Note that Garrett-Munk, and hence HWF, use an exponential profile for $N(z)$ and a broadband wavenumber-frequency spectrum of internal waves without steady currents. We use constant N and consider inertia waves and a steady current. Because the steady flow in (1) is geostrophic, the background density varies in y according to the thermal wind relation. Under present assumptions (constant R and the Boussinesq limit) such density variations leave N unchanged. The choice of constant R is reasonable for typical deep-ocean conditions, given that most of the short-wave groups in our simulations propagate less than a few hundred meters vertically and a few kilometers horizontally.

Ray tracing is used to follow short internal wave groups through the background given by (1). The short waves have wavenumber vector $\mathbf{k} = (k, 0, m)$, intrinsic frequency $\hat{\omega} = [(k^2N^2 + m^2f^2)/(k^2 + m^2)]^{1/2}$, and vertical component of the group velocity $c_g = \partial\hat{\omega}/\partial m$. The ray equations, integrated numerically, are $dz/dt = c_g$ and $dm/dt = -kU_z$, where $d/dt = \partial/\partial t + c_g\partial/\partial z$. Since the background is uniform in x, the horizontal wavenumber k remains constant along the ray. We choose $k = 2\pi(200m)^{-1}$, guided by HWF, who associate much of the dissipation in their model with about this horizontal scale.

HWF use a low-pass filter to remove temporarily from their background all waves whose vertical wavenumber ex-

[1]Department of Applied Mathematics, University of New South Wales, Sydney, Australia.
[2]Computational Physics Inc., Fairfax, VA.
[3]E.O. Hulburt Center for Space Research, Naval Research Laboratory, Washington, DC.
[4]Department of Applied Mechanics and Engineering Sciences, University of California, San Diego, La Jolla, CA.

1. REPORT DATE **SEP 1999**	2. REPORT TYPE	3. DATES COVERED **00-00-1999 to 00-00-1999**	
4. TITLE AND SUBTITLE **On the importance of weak steady shear in the refraction of short internal waves**		5a. CONTRACT NUMBER	
		5b. GRANT NUMBER	
		5c. PROGRAM ELEMENT NUMBER	
6. AUTHOR(S)		5d. PROJECT NUMBER	
		5e. TASK NUMBER	
		5f. WORK UNIT NUMBER	
7. PERFORMING ORGANIZATION NAME(S) AND ADDRESS(ES) **Naval Research Laboratory,E.O. Hulburt Center for Space Research,Washington,DC,20375**		8. PERFORMING ORGANIZATION REPORT NUMBER	
9. SPONSORING/MONITORING AGENCY NAME(S) AND ADDRESS(ES)		10. SPONSOR/MONITOR'S ACRONYM(S)	
		11. SPONSOR/MONITOR'S REPORT NUMBER(S)	
12. DISTRIBUTION/AVAILABILITY STATEMENT **Approved for public release; distribution unlimited**			
13. SUPPLEMENTARY NOTES			
14. ABSTRACT **see report**			
15. SUBJECT TERMS			

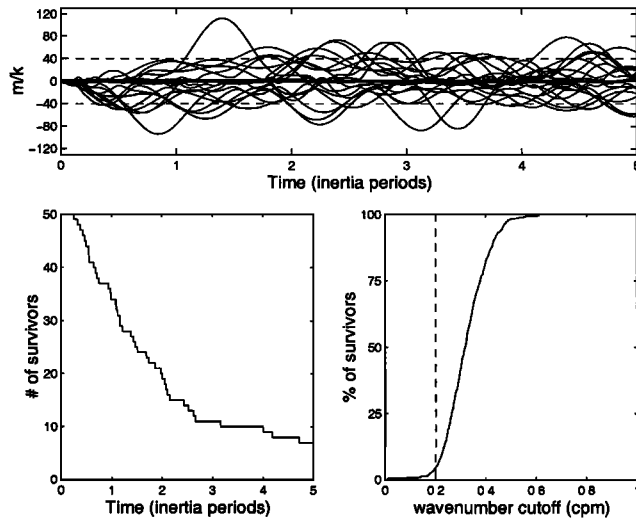| 16. SECURITY CLASSIFICATION OF:			17. LIMITATION OF ABSTRACT **Same as Report (SAR)**	18. NUMBER OF PAGES **4**	19a. NAME OF RESPONSIBLE PERSON
a. REPORT **unclassified**	b. ABSTRACT **unclassified**	c. THIS PAGE **unclassified**			

Figure 1. Top: ray solutions for vertical wavenumber along 20 of the 50 rays in a background given by (1) with $R = 0$. Dashed lines are $5m$ vertical wavelength. Lower left: the number of surviving rays as a function of time if the $5m$ cutoff is imposed. Lower right: the percentage of surviving rays after 5 inertia periods as a function of cutoff wavenumber.

ceeds the instantaneous vertical wavenumber m of the short-wave group. This is an attempt to satisfy the slowly-varying requirements of ray theory. We do not use such a filter. For one thing, our entire background would have had to be removed whenever a short-wave group reached a buoyancy-frequency turning point, where $m = 0$. More importantly, ray-theory validity in our model depends on the smallness of fractional changes in wavenumber, not on the magnitude of the wavenumber itself. For example, ray theory breaks down when fractional changes in wavenumber become large near caustics. Caustics can occur at any wavenumber of the short waves and cannot be eliminated from our simulations by filtering the background.

We shall often refer to a steady-shear critical-layer model. Specifically, we mean one in which $|m| \to \infty$ along the ray and in which $\hat{\omega} + kU(z)$ is constant – not just along the ray (guaranteed by the steadiness of the shear) but constant throughout space and time. From this constancy, it follows that

$$m^{-2}\partial m/\partial z \approx (-U_z/N)(1 - f^2/\hat{\omega}^2)^{-3/2} \qquad (2)$$

when $\hat{\omega} << N$, a result used below.

3. Results

We consider first the case without a steady current, i.e. $R = 0$ in (1). Figure 1, shows results for 50 ray integrations. In the upper panel, we plot the ray solution for vertical wavenumber along 20 of the 50 rays. Each ray integration is a different realization of (1). The initial condition is always $m = -1.4k$, or $\hat{\omega} \approx 15f$. The dashed line across the plot indicates the $5m$ wavelength. HWF terminate their ray integrations when $|m|$ exceeds this value, accounting crudely for dissipation. The lower left panel of Figure 1 shows the number of rays that would have survived had this wavenumber cutoff been imposed.

We ran experiments on sets of 50 ray integrations, imposing on each set a different cutoff wavenumber. Figure 1, lower right panel, shows the percentage of rays that survive the cutoff criterion after propagating for 5 inertia periods, as a function of cutoff wavenumber. The dashed vertical line represents a $5m$ cutoff. Doubling the cutoff wavelength to $10m$ makes little difference, in absolute terms, to survivability. However halving the cutoff wavelength to $2.5m$ increases the number of survivors by a factor of nearly 20.

We next add a steady current to the inertia-wave background. We choose R so that the steady-shear inverse Richardson number $R^2/N^2 = 0.01$ is small compared to the rms inverse Richardson number of 0.7 of the inertia waves. Repeating similar experiments to those of Figure 1 leads to the results of Figure 2.

The most rapid changes in vertical wavenumber are again due to refraction by the inertia waves, but now there is a gradual cumulative effect due to the steady shear. Calculation of the ensemble averaged vertical wavenumber $\langle m \rangle$ shows that it decreases approximately linearly with time, agreeing closely with the ray solution following one wave group in the steady shear only: $m(t) = m(t = 0) - kRt$. Thus the time t_c for $\langle m \rangle$ to reach some high-wavenumber cutoff m_c starting from $|m(t = 0)| << m_c$ is $t_c \approx m_c/kR$.

For the present parameter values and $m_c = 0.2$ cpm, t_c is only about 2.5 inertia periods, or about 43 hours. In HWF, the average short-wave survival time (the time it takes their short waves to refract to the cutoff wavenumber) is about 110 hours. In [Flatte, Henyey and Wright, 1985], whose ray-tracing model is the same as that of HWF, the characteristic time for the decay of wave-action (by refraction past the 5m cutoff) is about 170 hours. HWF and [Flatte, Henyey and Wright, 1985] use different initial conditions than we do, complicating a direct comparison of our results with theirs. They initialize the short waves with a range of intrinsic frequencies and a horizontal wavelength of $1000m$ compared to $200m$ here. However, their horizontal wavenumber spectra fill out quickly, with dissipation (i.e. refraction to the 5m cutoff vertical wavelength) peaking at a horizontal wavelength of about $200m$. Even at $1000m$ hor-
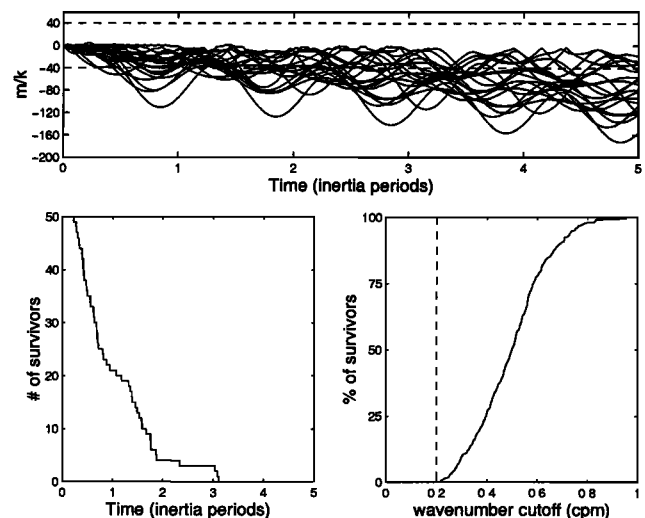

Figure 2. As in Figure 1 but for a background that includes a steady shear of strength $R = 0.1N$.
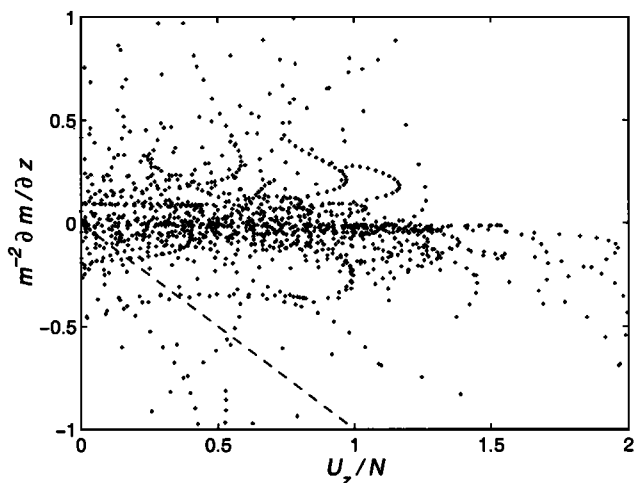
Figure 3. Scatter plot of the ray-divergence parameter versus U_z/N. Each point represents a value computed at equal time intervals along a ray path once the vertical wavelength decreases (and continues to decrease) below 10m.

izontal wavelength, our cutoff timescale t_c is comparable to the wave-action decay time of [*Flatte, Henyey and Wright*, 1985].

In fact, the timescale t_c is likely to overestimate the wave-action decay time in our results. This is because in determining $\langle m \rangle$ and t_c we did not apply a wavenumber cutoff to remove rays from the ensemble. Many of the rays will reach the cutoff well before the mean wavenumber does. If those rays are removed using a $5m$ cutoff wavelength, we obtain the results in the lower left panel of Figure 2. Here we see that all short-wave groups reach the cutoff in just over three inertia periods. The average survival time is less than one inertia period.

A proper comparison with HWF should incorporate three-dimensional effects omitted from the present model, such as short-wave transport in horizontal wavenumber, short-wave propagation normal to the current direction, and, in relation to the discussion below, ray divergence in three dimensions. These additional complications can be examined using the ray formulation presented in an on-line supplement[1] and conveniently expressed in variables that are non-singular at a caustic.

The lower right panel of Figure 2 is included as a warning that timescale estimates in this study, with and without steady-shear, increase as the cutoff wavelength decreases. If the cutoff wavelength is reduced to $2m$, nearly one-half of the rays in the example of Figure 2 survive after 5 inertia periods. Without mean shear, nearly all rays survive a $2m$ cutoff after 5 inertia periods, as indicated in Figure 1.

So far our ray integrations have considered a single ray at a time. The orientation of neighboring rays is also important, since it controls the change in wave-action density along the ray. HWF consider the density of wave-action in

phase space, where the coordinates include the wavenumber components and position. Wave-action density in phase space is constant along the trajectory through phase space, a result used by HWF to obtain estimates of internal-wave spectra.

We consider the space-time density of wave-action $A(\mathbf{x}, t)$, from which measures of linear instability (wave-steepness, perturbation shear) are easily computed along each ray. This wave-action density depends on the relative orientation of neighboring rays through the divergence of the group velocity vector: $dA/dt = -A\nabla \cdot \mathbf{c_g}$. Under present conditions we have $A(z, t)$ and

$$dA/dt = -A\Omega_{mm}\partial m/\partial z, \qquad (3)$$

where $\Omega(k, m, z, t) = \hat{\omega}(k, m) + kU(z, t)$.

The ray equation for $\partial m/\partial z$, obtained by differentiating the ray equation $dm/dt = -kU_z$ with respect to z, for the idealized situation considered here is

$$d/dt\,(\partial m/\partial z) = -kU_{zz} - \Omega_{mm}(\partial m/\partial z)^2. \qquad (4)$$

Using the approximate form for the internal-wave dispersion relation $\hat{\omega} \approx kN/|m|$, (3) becomes

$$(A\hat{\omega})^{-1}dA/dt = -2m^{-2}\partial m/\partial z. \qquad (5)$$

This shows that the fractional change in A over the time $\hat{\omega}^{-1}$ is proportional to $m^{-2}\partial m/\partial z$, the fractional change in m over a vertical distance of $|m|^{-1}$.

We call $m^{-2}\partial m/\partial z$ the ray-divergence parameter. It is positive when rays diverge, negative when rays converge, and infinite at a caustic and at a rotating critical layer (see (2)).

To proceed with the ray integrations we must specify an initial condition for $\partial m/\partial z$. In a critical-layer model the appropriate initial condition comes from (2). For our time-dependent shear we know of no obvious initial choice for
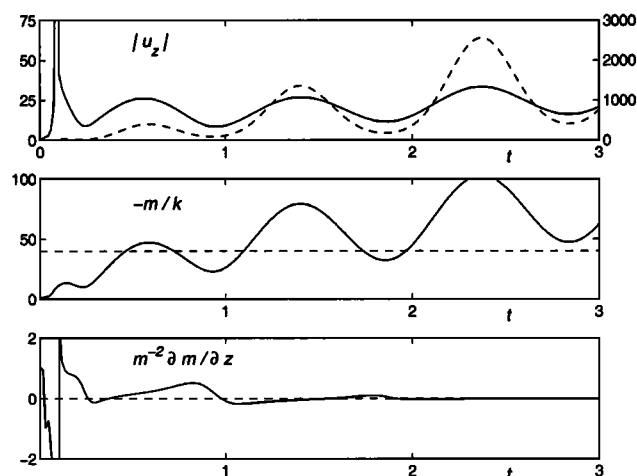

Figure 4. Sample ray-tracing solution. Each horizontal axis is time in inertia periods. Top: $|u_z|$ normalized by its initial value. The solid line (left axis) is the time-dependent ray solution. The spike at 0.09 inertia periods is a caustic. The dashed line (right axis) is for constant $c_g A$, with c_g obtained numerically. Middle: vertical wavenumber. Dashed line is $5m$ wavelength. Bottom: ray-divergence parameter.

$\partial m/\partial z$; so we simply initialize it using (2), though initializing to $\partial m/\partial z = 0$ does not alter the conclusions below.

Figure 3 shows a scatter plot of $m^{-2}\partial m/\partial z$ versus U_z/N for 20 ray integrations. The data points are restricted to values for which the vertical wavelength of the short waves is less than $10m$ and is decreasing. We choose wavelengths shorter than $10m$ because dissipative processes are believed to be important at these scales. Modified forms of (3) and (4) were integrated, which are not singular at caustics (see [Broutman, 1986]). Parameter values and initial conditions are the same as in Figure 2.

The dashed line in Figure 3 is $m^{-2}\partial m/\partial z = -U_z/N$. For the steady-shear critical-layer problem, $m^{-2}\partial m/\partial z$ is constrained to be below this line (or on it if $f = 0$, see (2)). For our combination of inertia and steady shear, almost all of the data points lie above this line, indicating that at short vertical scale, the strength of ray convergence is almost always weaker than in a steady-shear critical-layer encounter. In nearly half of the data points, the rays actually diverge as they refract to small scale. In the majority of cases, the wave-energy density $\hat{\omega}A$ decreases with increasing vertical wavenumber, contrary to behavior in a steady-shear critical-layer encounter. Conditions of weak convergence in time-dependent shear were also reported by [Broutman et al., 1997] and by [Eckermann, 1997], but for a simpler background consisting of one long wave.

The effect of weak ray-convergence on a short-wave shear amplitude, $|u_z|$, is shown in Figure 4. Here u is the x–component of the perturbation velocity due to the short waves, so $|u_z| = |mu|$ represents the magnitude of a perturbation shear, an important indicator of instability. In the upper panel, the solid line (left axis) is computed from the ray-tracing solution for wave-action density. The dashed line (right axis) is computed by regarding wave-action flux c_gA as constant, as is sometimes assumed in steady-shear refraction models. The point of the plot is to illustrate that the growth in $|u_z|$ (top panel) with increasing vertical wavenumber (middle panel) can be quite modest in time-dependent shear due to weak ray convergence (lower panel). For example, from 1.85 to 2.4 inertia periods $-m/k$ increases by a factor of about 3.2. The corresponding factor of increase in $|u_z|$ is 14.5 when assuming constant c_gA but only 2.9 for the full ray-tracing solution.

4. Discussion

The first point to make is that although the inertia waves in this study generate much stronger shears than the steady

current, the steady current contributes a gradual but important cumulative component to the refraction. The persistence of the steady shear compensates for its weak strength.

The second point to make is that our results show variability in the strength of ray convergence as the short waves refract to small vertical scales. The ray paths are almost as likely to diverge as converge, and when they do converge, they are unlikely to converge as strongly as in a conventional critical layer interaction. There remains the interesting possibility that the presence of weak steady shear in an internal-wave background has partially counter-acting effects on the mixing rate: it may speed up short-wave transport to small scales, but it may also delay short-wave instability by weakening the convergence.

References

Broutman, D., On internal-wave caustics. J. Phys. Oceanogr. 16, 1625–1635, 1986.

Broutman, D., C. Macaskill, M. E. McIntyre, and J. Rottman, On Doppler-spreading models of internal waves. Geophys. Res. Lett. 24, 2813–2816, 1997.

Eckermann, S. D., Influence of wave propagation on the Doppler-spreading of atmospheric gravity waves. J. Atmos. Sci. 54, 2554-2573, 1997.

Flatte, S.M., F.S. Henyey, and J. Wright, Eikonal calculations of short-wavelength internal-wave spectra. J. Geophys. Res. 90, 7265-7272, 1985.

Gregg, M.C., D.P. Winkel, T.B. Sanford, and H. Peters, Turbulence produced by internal waves in the oceanic thermocline at mid and low latitudes. Dyn. Atmos. Oceans. 24, 1-14, 1996.

Henyey, F. S., J. Wright, and S. M. Flatte, Energy and action flow through the internal wave field: an eikonal approach. J. Geophys. Res. 91, 8487-8495, 1986.

Munk, W. H., Internal waves and small-scale processes. In Evolution of Physical Oceanography (ed. B. A. Warren and C. Wunsch), p. 623, MIT Press, 1981.

D. Broutman and S. Eckermann, E.O. Hulburt Center for Space Research, Naval Research Laboratory, Code 7641, Washington DC 20375-5352. (e-mail: daveb@power.nrl.navy.mil; eckerman@ismap4.nrl.navy.mil)

G. Buckley, Department of Applied Mathematics, University of New South Wales, Sydney, NSW, 2052, Australia. (e-mail: g.buckley@unsw.edu.au)

J. W. Rottman, Department of Applied Mechanics and Engineering Sciences, University of California, San Diego, 9500 Gilman Drive, La Jolla, CA 92093-0411. (e-mail: jrottman@ames.ucsd.edu)